nature astronomy

Article

https://doi.org/10.1038/s41550-024-02258-z

Asteroid Kamo'oalewa's journey from the lunar Giordano Bruno crater to Earth 1:1 resonance

In the format provided by the authors and unedited

Asteroid Kamo‘oalewa’s Journey from Lunar Giordano Bruno Crater to Earth 1:1 Resonance

Yifei Jiao, Bin Cheng, Yukun Huang, Erik Asphaug, Brett Gladman, Renu Malhotra, Patrick Michel, Yang Yu & Hexi Baoyin

Supplementary Information

This PDF file includes:

Supplementary Text
Supplementary Figs. 1 to 8
Supplementary Tables 1 to 5
References

Supplementary Text

Different lunar impact conditions. Given a specific lunar crater, it is difficult to constrain the associated impact event strictly, since different impact conditions may result in similar crater morphology and ejecta deposition. Here we test the influence of different impact conditions, varying the impact velocities from 15 km/s to 24 km/s and the incident angles in 30°–60° from the surface horizon, as shown in Supplementary Table 1 and Supplementary Figs. 1–5. For each case, the impactor size is estimated using the scaling law as described in the Methods section, assuming the same final crater size as the Kepler crater to constrain the Weibull parameters. Note that the Weibull parameters m and k are not wholly independent constants. Typically, rocks with equal $\ln(kV)/m$ tend to have similar overall disruption thresholds, where V is the rock volume. A smaller Weibull k denotes a material with fewer cracks, making it more resistant to shock damage, thereby producing larger fragments upon impact[22, 68]. Throughout all the impact conditions investigated in this work, we find that the Weibull parameters $m = 9.5$ and $k = 10^{30}$–10^{33} m^{-3} are good fits to the upper limit of the Kepler fragment size-velocity distribution[16], and give similar results for the largest escaping fragment sizes that are approximately 2.5%–5.6% of the impactor size. We then estimate the required crater diameter to produce Kamo'oalewa-sized (36 m) escaping fragments using the scaling law, which suggests a range of 8.2 km to 21.4 km (close to the 10–20 km used in the main text). Different impact conditions also affect the number of escaping fragments (>36 m), which determines the number of launched particles in the N-body simulations. For the GB crater, the launch number is estimated using a linear relation to the impactor's volume (see Methods). In particular, the result deviations for different impact velocities are always within ±20% when the impact angle is fixed at 45°. While the ejection results are more affected by the impact angles. The number of fragments (faster than lunar escape velocity and larger than 36 m) from a 60° impact is about 30% of that from the 45° case; for a more oblique 30° impact, the number is about twice as high. This trend is consistent with prior works focused on high-velocity oblique impacts on the Martian surface[69]. Finally, the ultimate Kamo'oalewa-like object number is determined by multiplying the Earth co-orbital fraction with the number of launch fragments. With a maximum fraction of 1% as described in the main text, we can expect about 0.2–2.4 (when $k = 10^{33}$ m^{-3}) or 2.3–7.9 ($k = 10^{30}$ m^{-3}) Earth co-orbitals from the GB crater. To summarize, varying lunar impact conditions leads to ejection results of the same order of magnitude, and thus has minor effects on the required crater size and Earth co-orbital outcomes.

Supplementary Table 1: Simulation results for different lunar impact conditions. The nominal 18 km/s and 45° case is expected to be more frequent than other cases. The number of Earth co-orbitals is estimated using a maximum fraction of about 1% as described in the main text.

Impact velocity (km/s)	15	18	**18**	18	21	24
Impact angle from surface horizon (°)	45	30	**45**	60	45	45
Impactor diameter for a 31-km crater (m)	2696	2952	2440	2182	2242	2082
Largest escaping fragment size (m)	82–142	101–163	62–112	54–81	67–109	64–117
Largest escaping fragment size over impactor size	0.030–0.053	0.034–0.055	0.025–0.046	0.025–0.037	0.030–0.049	0.031–0.056
Number of escaping fragments >36 m	266–1447	754–2511	296–1249	60–401	243–1013	233–1036
Required crater diameter for 36-m escaping fragments (km)	9.1–15.1	8.2–12.5	11.3–19.4	15.2–21.4	11.5–17.8	10.9–18.5
Number of escaping fragments >36 m from GB	83–453	236–786	93–391	19–126	76–317	73–324
Maximum number of Earth co-orbitals from GB	0.8–4.5	2.4–7.9	0.9–3.9	0.2–1.3	0.8–3.2	0.7–3.2

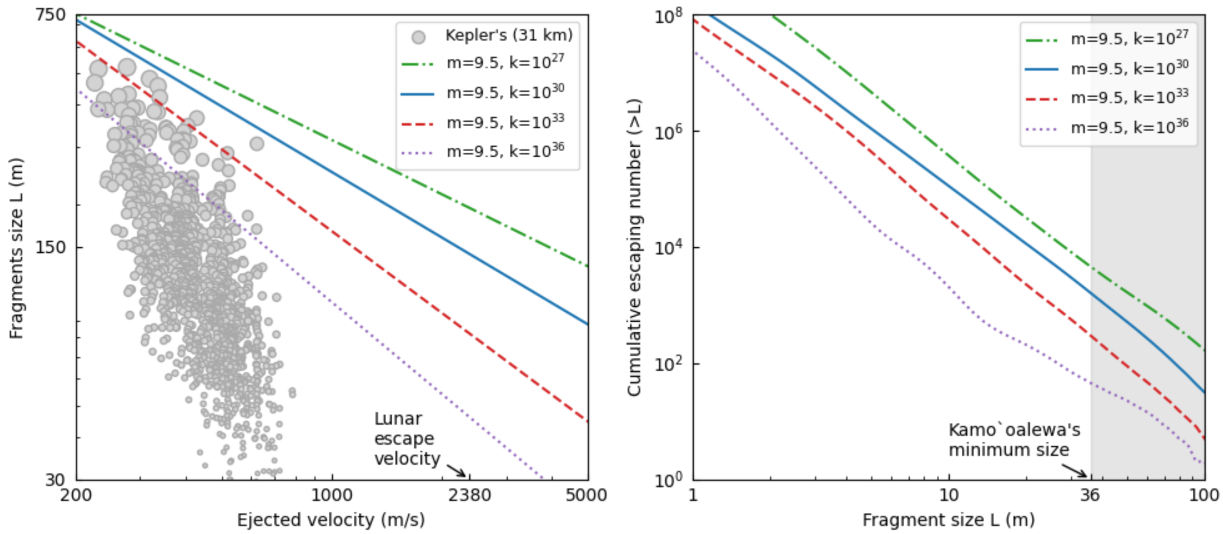

Supplementary Fig. 1: Same as Fig. 2 in the main text, but for impact velocity of 15 km/s at 45°. In the left panel, the lines represent the largest fragment sizes versus ejected velocities with different Weibull parameters, fitted as a simple power law. The circle points are computed from the secondary craters of the Kepler crater[16], which has a cutoff at about 800 m/s due to the difficulty in searching secondaries at great distances. The upper limit of the Kepler's fragment size-velocity distribution helps us to estimate the Weibull parameters. In the right panel, we present the cumulative size-frequency distribution of ejected fragments with velocities faster than lunar escape velocity.

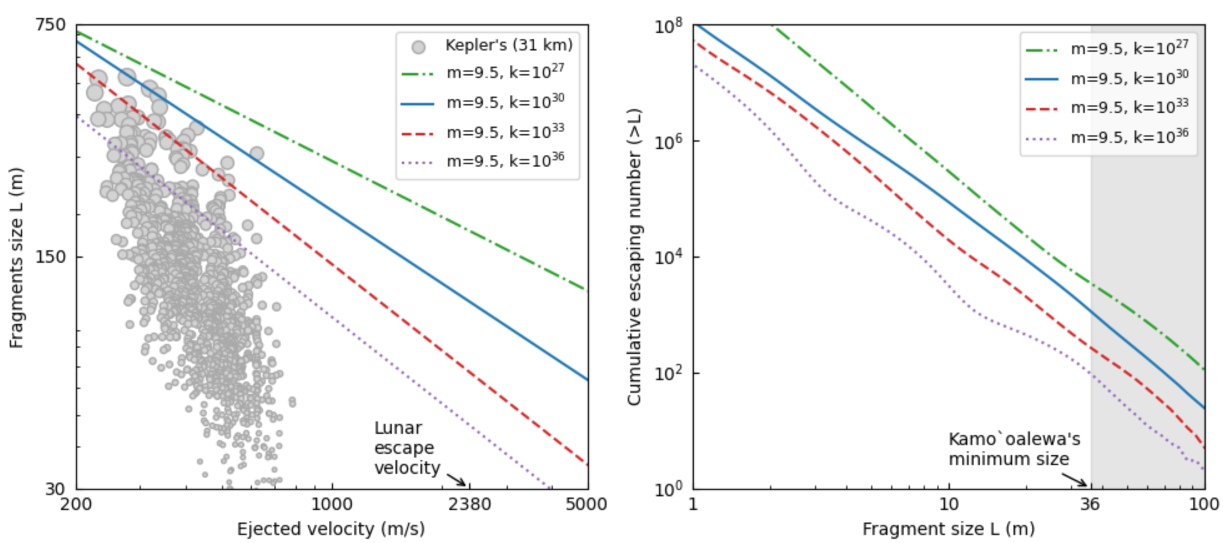

Supplementary Fig. 2: Same as Fig. 2 in the main text, but for impact velocity of 21 km/s at 45°.

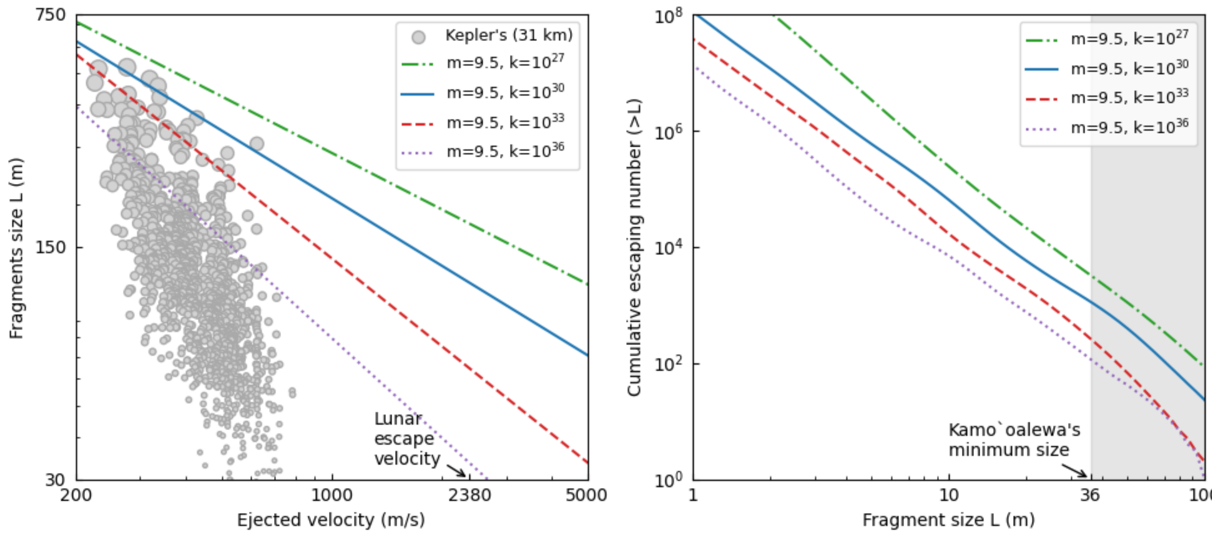

Supplementary Fig. 3: Same as Fig. 2 in the main text, but for impact velocity of 24 km/s at 45°.

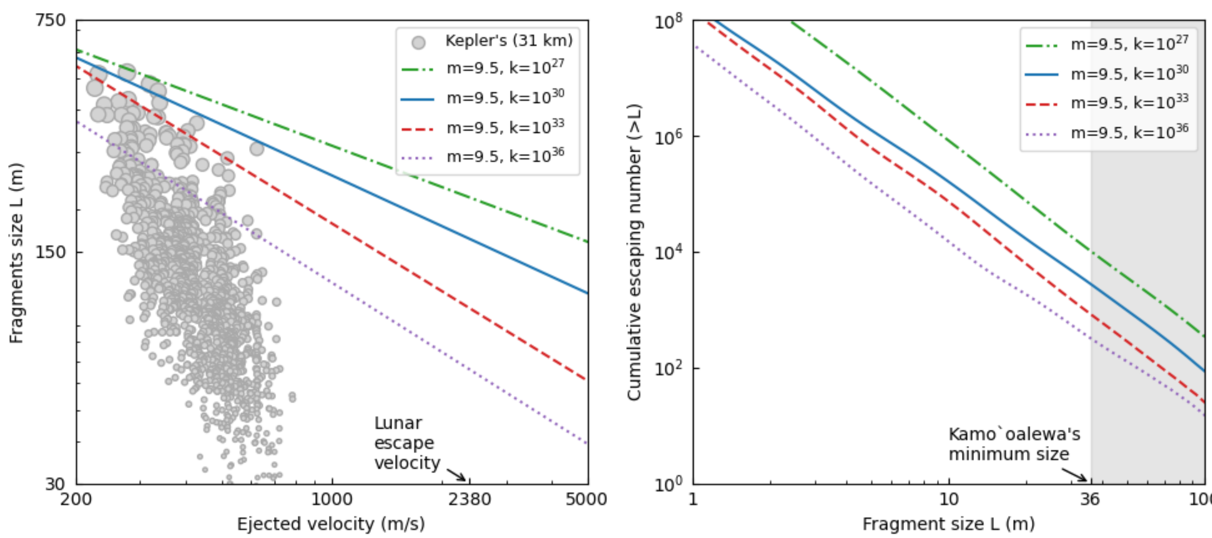

Supplementary Fig. 4: Same as Fig. 2 in the main text, but for impact velocity of 18 km/s at 30°.

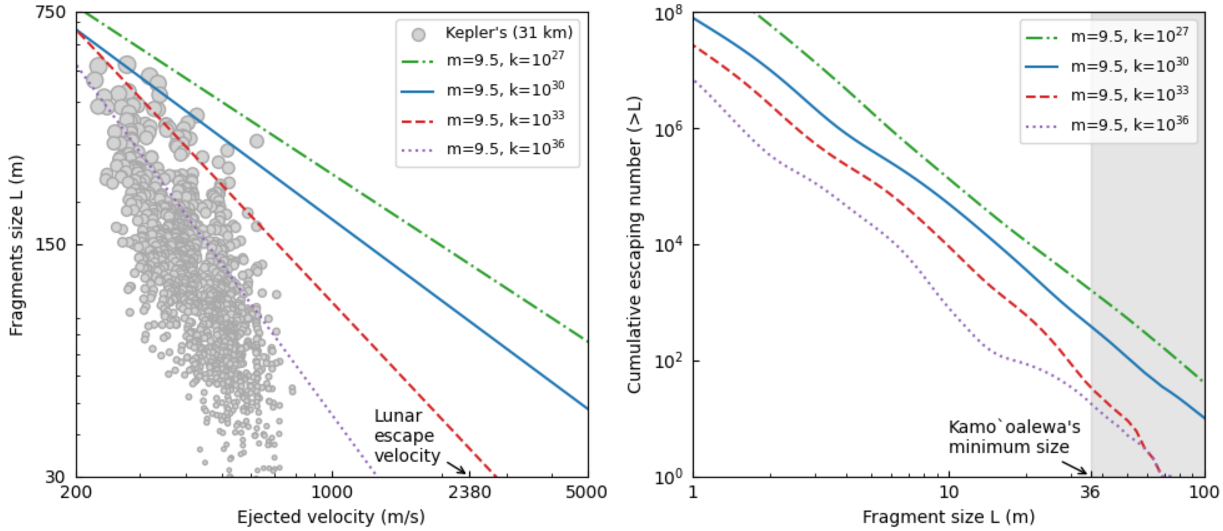

Supplementary Fig. 5: Same as Fig. 2 in the main text, but for impact velocity of 18 km/s at 60°.

Supplementary Table 2: List of source crater candidates for asteroid Kamo'oalewa[34]. Since the errors in crater ages are not fully reported[34], we have included some published model errors here[36, 72, 35].

Name	D (km)	Age (Myr)	Name	D (km)	Age (Myr)
Tycho	85	109 ± 4[36]	(No name)	13	26
Jackson	71	147 −24/+23[72]	Egede A	13	84
Necho	37	80 ± 24[35]	(No name)	13	113
Thales	32	61	(No name)	12	145
Moore F	24	41 ± 12[35]	(No name)	12	81
Giordano Bruno	22	4 −3/+6[35]	(No name)	12	54
Byrgius A	19	47 ± 14[35]	Furnerius A	12	29
Sundman V	18	93	(No name)	11	39
Mandel'shtam F	16	44	(No name)	11	126
Ryder	16	140	Avery	11	139
Rayet Y	15	40	Messier A	11	128
(No name)	15	138	(No name)	11	137
(No name)	15	31	Euclides C	11	50
Fechner T	15	33	(No name)	11	13
(No name)	14	56	(No name)	10	110
Tharp	14	22	(No name)	10	34

Supplementary Table 3: GB escaping particles N-body simulation results.

Total Runtime	10 Myr		100 Myr	
Phase	Geo	Helio	Geo	Helio
Launch particles	60,000	50,581	6,000	5,014
Survivals	50,581	10,584	5,014	44
Collisions[a]				
Earth	8,863	27,857	929	2,942
Moon	556	-	57	-
Venus	-	9,878	-	1,315
Mercury	-	276	-	71
Mars	-	170	-	42
$Q > 6.0$ au[b]	-	578	-	163
$q < 0.01$ au[b]	-	1,238	-	437

[a] In geocentric phase, collisions with Earth and Moon are considered separately; while in heliocentric phase, the Earth-Moon system is treated as a whole at their barycenter.

[b] Q for aphelion and q for perihelion.

Supplementary Table 4: Material parameters for SPH simulations.

Model	Description	Parameter	
Tillotson EOS[22]	Bulk density	ρ (kg/m^3)	2,700
	Bulk modulus	A_T (Pa)	2.67×10^{10}
	Tillotson parameter	B_T (Pa)	2.67×10^{10}
	Tillotson parameter	a_T	0.5
	Tillotson parameter	b_T	1.5
	Tillotson parameter	α_T	5.0
	Tillotson parameter	β_T	5.0
	Tillotson parameter	e_0 (J/kg)	4.87×10^8
	Incipient vaporization energy	e_{IV} (J/kg)	4.72×10^6
	Complete vaporization energy	e_{CV} (J/kg)	1.82×10^7
Strength model[70]	Shear modulus	G (Pa)	2.27×10^{10}
	Strength limit	Y_m (Pa)	2.49×10^9
	Cohesive strength (intact)	$Y_{0,i}$ (Pa)	3.19×10^7
	Cohesive strength (damaged)	$Y_{0,d}$ (Pa)	1.0×10^4
	Frictional coefficient (intact)	μ_i	1.1
	Frictional coefficient (damaged)	μ_d	0.71
Fracture model[71]	Weibull exponent	m	9.5
	Weibull coefficient	k (m^{-3})	10^{27}, 10^{30}, 10^{33}, 10^{36}

Supplementary Table 5: Coefficients of the fitted function for Earth co-orbital fraction, as described by Eq. (7) in Methods.

	α_3	α_2	α_1	α_0
Mean	-0.05289417	-0.05226572	-0.08133859	-5.84075464
M+1SD	-0.05315579	-0.04016629	-0.02382655	-5.32263352
M+2SD	-0.05375852	-0.03574631	0.00052753	-4.98426973
M+3SD	-0.05413179	-0.03352175	0.01378271	-4.73206501

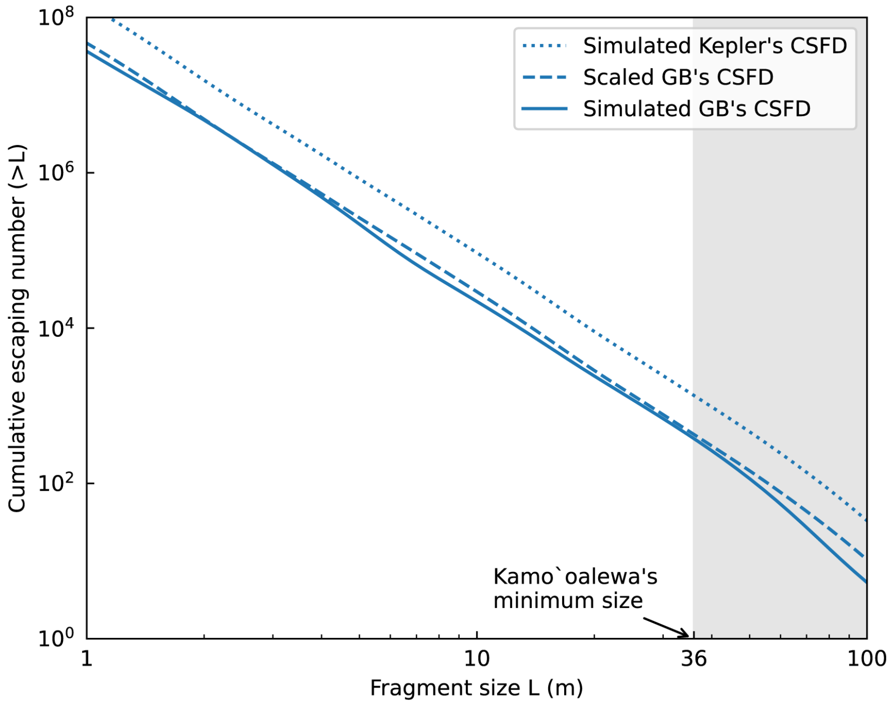

Supplementary Fig. 6: Simulated escaping fragment CSFD from a GB-sized crater. Here we present SPH result for a GB-sized crater (solid line), adopting k of 10^{30} m^{-3} and m of 9.5, which is similar to the scaled result (dashed line) computed from Eq. (5) in Methods. The simulated result of a Kepler-sized crater (dotted line) is used as a baseline.

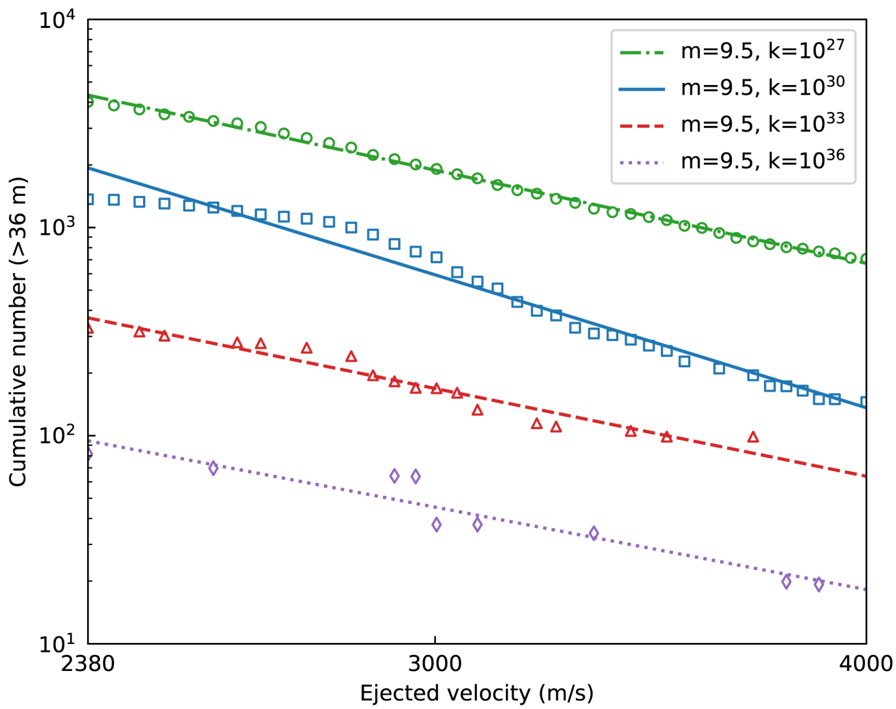

Supplementary Fig. 7: Large fragments (>36 m) cumulative velocity frequency distribution from a Kepler-sized crater. The cumulative number of large escaping fragments follows a power-law dependency over their velocities with a power of about −4.0, so that most of them are ejected slightly faster than lunar escape velocity. ∼90% are launched from 2.38 to 4.0 km/s, and ∼98% are launched from 2.38 to 6.0 km/s, which is consistent with previous works[21].

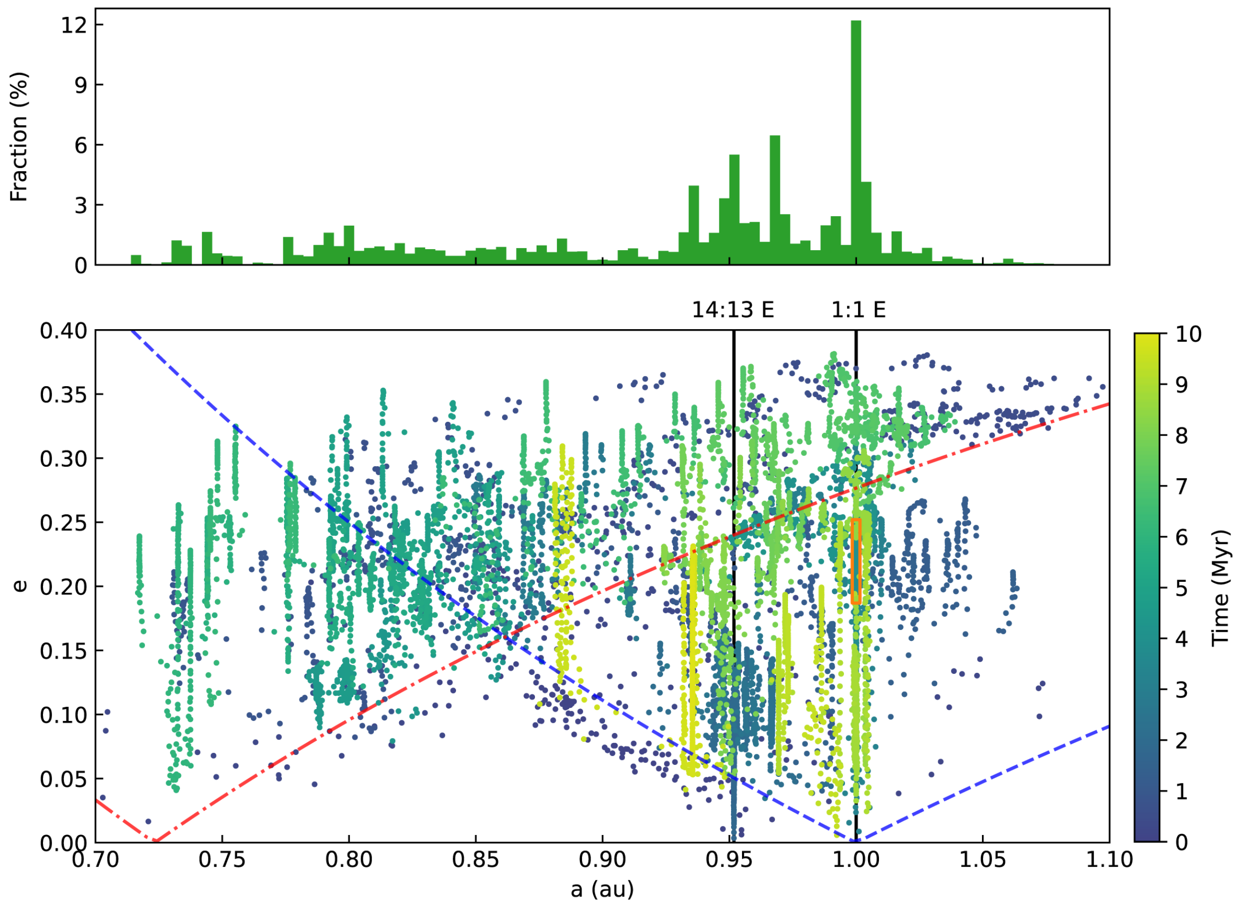

Supplementary Fig. 8: Orbital evolution example of an individual particle. The points represents the particle's orbital states at different times (with a 1 kyr interval). The orange box from 3.33 to 3.375 Myr has been plotted in Fig. 3a for Earth co-orbital details. The two dashed lines indicate $a(1 \pm e) = a_{\rm Earth}$ or $a_{\rm Venus}$. Note that this particle may switch between different resonance ratios over time, including Earth co-orbital (~12% of its lifetime) and some other resonant ratios, e.g., the temporary 14:13 resonance with Earth, as indicated by the black solid lines.

References

[16] Singer, K. N., Jolliff, B. L. & McKinnon, W. B. Lunar secondary craters and estimated ejecta block sizes reveal a scale-dependent fragmentation trend. *J. Geophys. Res.: Planets* **125**, e2019JE006313 (2020).

[21] Artemieva, N. & Shuvalov, V. Numerical simulation of high-velocity impact ejecta following falls of comets and asteroids onto the Moon. *Sol. Syst. Res.* **42**, 329 (2008).

[22] Benz, W. & Asphaug, E. Simulations of brittle solids using smooth particle hydrodynamics. *Comput. Phys. Commun.* **87**, 253–265 (1995).

[34] Mazrouei, S., Ghent, R. R., Bottke, W. F., Parker, A. H. & Gernon, T. M. Earth and Moon impact flux increased at the end of the Paleozoic. *Science* **363**, 253–257 (2019).

[35] Morota, T. *et al.* Formation age of the lunar crater Giordano Bruno. *Meteorit. Planet. Sci.* **44**, 1115–1120 (2009).

[36] Drozd, R., Hohenberg, C., Morgan, C., Podosek, F. & Wroge, M. Cosmic-ray exposure history at Taurus-Littrow. In *Lunar Science Conference* (1977).

[68] Benz, W. & Asphaug, E. Impact simulations with fracture. I. method and tests. *Icarus* **107**, 98–116 (1994).

[69] Artemieva, N. & Ivanov, B. Launch of Martian meteorites in oblique impacts. *Icarus* **171**, 84–101 (2004).

[70] Potter, R. W., Collins, G. S., Kiefer, W. S., McGovern, P. J. & Kring, D. A. Constraining the size of the South Pole-Aitken basin impact. *Icarus* **220**, 730–743 (2012).

[71] Wiggins, S. E., Johnson, B. C., Bowling, T. J., Melosh, H. J. & Silber, E. A. Impact fragmentation and the development of the deep lunar megaregolith. *J. Geophys. Res.: Planets* **124**, 941–957 (2019).

[72] Van der Bogert, C. *et al.* Discrepancies between crater size-frequency distributions on ejecta and impact melt pools at lunar craters: An effect of differing target properties? In *41st Annual Lunar and Planetary Science Conference*, 1533, 2165 (2010).